Article

Conductive Sub-micrometric Wires of Platinum-Carbonyl Clusters Fabricated by Soft-Lithography

Pierpaolo Greco, Massimiliano Cavallini, Pablo Stoliar, Santiago David Quiroga, Soumya Dutta, Stefano Zacchini, Maria Carmela Iapalucci, Vittorio Morandi, Silvia Milita, Pier Giorgio Merli, and Fabio Biscarini

J. Am. Chem. Soc., **2008**, 130 (4), 1177-1182 • DOI: 10.1021/ja074104m

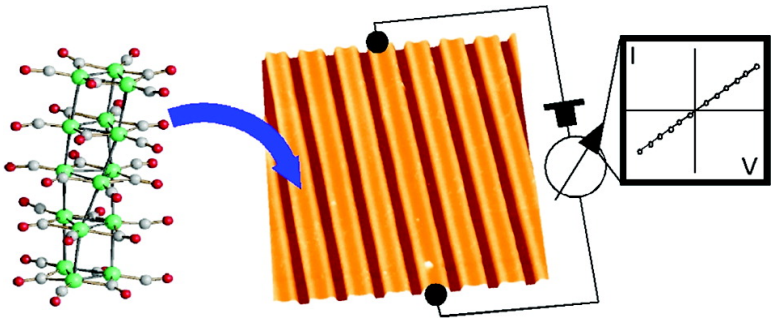

More About This Article

Additional resources and features associated with this article are available within the HTML version:

- Supporting Information
- Links to the 5 articles that cite this article, as of the time of this article download
- Access to high resolution figures
- Links to articles and content related to this article
- Copyright permission to reproduce figures and/or text from this article

View the Full Text HTML

J|A|C|S
ARTICLES
Published on Web 01/09/2008

Conductive Sub-micrometric Wires of Platinum-Carbonyl Clusters Fabricated by Soft-Lithography

Pierpaolo Greco,[†] Massimiliano Cavallini,*[,†] Pablo Stoliar,[†] Santiago David Quiroga,[†] Soumya Dutta,[†] Stefano Zacchini,[‡] Maria Carmela Iapalucci,[‡] Vittorio Morandi,[§] Silvia Milita,[§] Pier Giorgio Merli,[§] and Fabio Biscarini*[,†]

CNR-ISMN Bologna, Via P. Gobetti 101, I-40129 Bologna, Italy, Dipartimento di Chimica Fisica e Inorganica, Università di Bologna, V.le Risorgimento 4, 40136 Bologna, Italy, and CNR-IMM Bologna, Via P. Gobetti 101, I-40129 Bologna, Italy

Received June 6, 2007; E-mail: m.cavallini@bo.ismn.cnr.it; f.biscarini@bo.ismn.cnr.it

Abstract: Conductive wires of sub-micrometer width made from platinum-carbonyl clusters have been fabricated by solution-infilling of microchannels as in microinject molding in capillaries (MIMIC). The process is driven by the liquid surface tension within the micrometric channels followed by the precipitation of the solute. Orientation of supramolecular crystalline domains is imparted by the solution confinement combined with unidirectional flow. The wires exhibit ohmic conductivity with a value of 0.2 S/cm that increases, after thermal decomposition of the platinum-carbonyl cluster precursor to Pt, to 35 S/cm.

Introduction

A major effort in nanotechnology has been devoted to the patterning of active materials into size and shape controlled structures, to achieve the ambitious goal of controlling physical properties through the control of materials at different length scales.[1] However, the interconnection of active nanostructures with the macroscopic world is still an open problem that severely limits many applications. In order to connect systems across length scales, technology requires easily processable highly conductive wires that are stable under ambient conditions. Noble metals, such as Au and Pt, widely used in microelectronics, are ideal candidates for these purposes due to stability versus oxidation combined with a high conductivity.

Several methods have been proposed for fabricating highly conductive micro- and nanowires. Among them, in situ controlled deposition of metal−organic precursors from vapor phase, followed by Focused Ion Beam (FIB)[2] or Electron-Beam (EB)[3] decomposition, are quite effective, widely adopted in laboratory research. However the apparatus required are expensive and the technique is difficult to upscale, which limit their technological application.

A breakthrough approach involves material precursors, which can be processed and patterned from solutions, viz. within the same technological platform as organic semiconductors.[4] Examples include Ag[5] or Au[6] nanorods, Cu and FeS[7] nanowires, and metal oxides semiconductors.[8]

Here we propose the use of solution processable metal carbonyl clusters for conductive nanowires. They offer the possibility to process several metals or even combinations (alloys) of different metals from a variety of solvents and mild curing conditions. Evidence supporting this approach comes from solution casting of water/2-propanol solutions of $[Pt_{3n}(CO)_{6n}]^{2-}$ ($n = 4-6$) on several substrates which yields the preferential formation of Pt nanowires over other morphologies.[9] Moreover, as inferred from TEM images, well-defined Pt morphologies, including Pt nanowires, have also been obtained by preparing $[Pt_{3n}(CO)_{6n}]^{2-}$ ($n = 4-6$) dianions in the micropores of zeolites, followed by thermal decomposition.[10] Nonetheless, both of these approaches do not yield the formation of ordered structures. Here the problem of promoting a controlled highly ordered assembly of metal clusters is overcome by confining the deposition of Pt carbonyl clusters with the use of stamps[11,12]

[†] CNR-ISMN Bologna.
[‡] Università di Bologna.
[§] CNR-IMM Bologna.

(1) Cavallini, M.; Stoliar, P.; Moulin, J. F.; Surin, M.; Leclère, P.; Lazzaroni, R.; Breiby, D. W.; Andreasen, J. W.; Nielsen, M. M.; Sonar, P.; Grimsdale, A. C.; Müllen, K.; Biscarini, F. *Nano Lett.* **2005**, *5*, 2422−2425.
(2) Rotkina, L.; Oh, S.; Eckstein, J. N.; Rotkin, S. V. *Phys. Rev. B* **2005**, *72* (23), 1−4.
(3) Rotkina, L.; Lin, J. F.; Bird, J. P. *Appl. Phys. Lett.* **2003**, *83* (21), 4426−4428.
(4) Rao, C. N. R.; Deepak, F. L.; Gundiah, G.; Govindaraj, A. *Prog. Solid State Chem.* **2003**, *31*, 5−147.
(5) (a) Gunawidjaja, R.; Jiang, C. Y.; Ko, H. H.; Tsukruk, V. V. *Adv. Mater.* **2006**, *18* (21), 2895. (b) Hong, B. H.; Bae, S. C.; Lee, C. W.; Jeong, S.; Kim, K. S. *Science* **2001**, *294* (5541), 348. (c) Zhang, S. H.; Jiang, Z. Y.; Xie, Z. X.; Xu, X.; Huang, R. B.; Zheng, L. S. *J. Phys. Chem. B* **2005**, *109*, 9416.
(6) Mieszawska, A. J.; Slawinski, G. W.; Zamborini, F. P. *J. Am. Chem. Soc.* **2006**, *128*, 5622 − 5623.
(7) (a) Judai, K.; Nishijo, J.; Nishi, N. *Adv. Mater.* **2006**, *18* (21), 2842−. (b) Wang, W.; Wang, S. Y.; Wang, K. Y.; Gao, Y. L.; Liu, M. *Sol. State Commun.* **2006**, *140* (7−8), 325−328.
(8) (a) Lee, S. H.; Lee, H. J.; Oh, D.; Lee, S. W.; Goto, H.; Buckmaster, R.; Yasukawa, T.; Matsue, T.; Hong, S. K.; Ko, H.; Cho, M. W.; Yao, T. F. *J. Phys. Chem. B* **2006**, *110*, 3856. (b) Su, C. Y.; Goforth, A. M.; Smith, M. D.; Pellechia, P. J.; zur Loye, H. C. *J. Am. Chem. Soc.* **2004**, *126*, 3576−3586.
(9) Remita, H.; Keita, B.; Torigoe, K.; Belloni, J.; Nadjo, L. *Surf. Sci.* **2004**, *572*, 301−308.
(10) Ichikawa, M. In *Metal Clusters in Chemistry*; Braunstein, P.; Oro, L. A.; Raithby, O., Eds.; Wiley-VCH, Weinheim, 1999; Vol. 3, pp 1273−1301.
(11) Xia, Y.; Whitesides, G. M. *Angew. Chem., Int. Ed.* **1998**, *37* (5), 551−575.
(12) (a) Cavallini, M.; Biscarini, F. *Nano Lett.* **2003**, *3* (9), 1269−1271. (b) Cavallini, M.; Murgia, M.; Biscarini, F. *Nano Lett.* **2001**, *1*, 193−195.

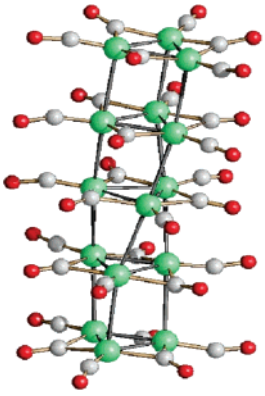

(1)

Figure 1. Molecular structure of the $[Pt_{15}(CO)_{18}]^{2-}$ cluster anion. Green are the platinum atoms, gray are the carbon atoms, red are the oxygen atoms.

therefore changing the degrees of freedom and the time scales of the deposition.

Here we propose the application of Microinject Molding in Capillaries[13,14] to obtain a pattern of sub-micrometric stripes (μ-stripes) of the Pt carbonyl clusters $[NBu_4]_2[Pt_{15}(CO)_{30}]$, and we compared its conductive properties with continuous thin solid films.

Furthermore the Pt carbonyl μ-stripes are turned into metallic Pt nanowires after thermal decomposition. Decomposition of the platinum-carbonyl and precipitation of structured crystals from different solutions have been studied in sub-micrometric channels.

Results and Discussion

The molecular precursor employed in this work for the fabrication of Pt wires is the $[NBu_4]^+$ salt of the $[Pt_{15}(CO)_{30}]^{2-}$ (**1**) cluster anion (Figure 1) for several reasons. First, it can be easily synthesized in water from commercial Pt salts, as recently reported.[15] Moreover, molecular species, depending on the cluster size and the nature of the counterion, self-assemble upon crystallization to yield molecular wires,[16] which are organized into 1-D, 2-D, or 3-D structures.

Films. Films of **1** were prepared by drop casting 20 μL of its solution (0.6 g/L) in dimethylformamide (DMF) or tetrahydrofuran (THF) on glass.

The nature of the deposited materials largely depends on the experimental conditions. Micro-IR experiments on samples obtained by drop casting in air show that the deposited material retains its molecular carbonyl nature when volatile solvents such as THF or acetone are used. Conversely, when a less volatile solvent such as DMF is employed, the Pt-carbonyl clusters decompose during evaporation in air to give Pt colloids, which are contaminated by organic species, arising from the tetra-alkyl ammonium cations. This solvent-dependent decomposition behavior is not observed when depositing the cluster solutions under a nitrogen flow; in this case, in fact, the deposited material always retains the carbonyl molecular nature of the precursor, independently of the solvent used. Moreover, the samples grown under a nitrogen atmosphere show rod-like crystals, which are more than 50 μm long with an aspect ratio of >10:1 (see Figure 2a).

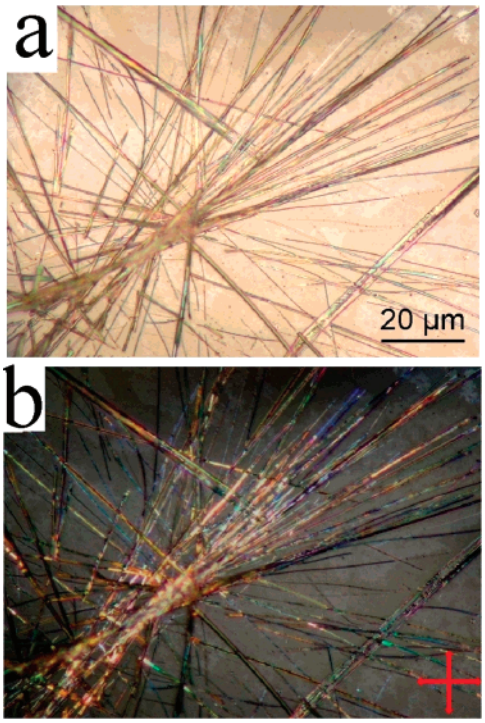

Figure 2. Optical micrographs (magnification 50×) of **1** on glass after deposition under nitrogen. (a) Micrographs taken under unpolarized light. (b) Micrographs taken with crossed polars oriented along the axes of the image.

The observation under crossed polars (Figure 2b) shows the typical behavior of optically anisotropic materials; i.e., the crystals appear colored under crossed polars, where the colors range from green to yellow depending on the local thickness. Evidence of light extinction in regions of the crystals indicates that each crystal is formed by several domains, whose length ranges between 2 μm and 15 μm. No evidence of preferential orientation of these domains is observed.

On the other hand, the samples grown in air appear inhomogeneous and very rough; no sign of birifringence has been observed by optical microscope. The different appearance of the samples deposited under nitrogen compared to the ones obtained in air is consistent with the fact that these compounds are air-sensitive in solution. The decomposition of **1** is confirmed by the spectroscopic evidence that **1** loses its molecular carbonyl nature when deposited in air. In all cases, thermal treatment in air at temperatures higher than 100 °C decomposes the carbonyl clusters removing completely the organic components. Thermogravimetric Analysis (TGA), shown in Figure 3, clearly indicates that already at ca. 100 °C all the carbonyl ligands and the $[NBu_4]^+$ cations are removed from **1** leaving only metallic Pt.

Patterning of Sub-micrometric Stripes. The sub-micrometric stripes of **1** have been fabricated by Microinject Molding In Capillaries (MIMIC),[13] whose scheme is shown in Figure 4. A stamp made of polydimethylsiloxane (PDMS), whose motif consists of parallel protruding lines (125 nm thick, 300 nm width and 740 nm pitch), is placed in contact with the surface. The grooves between the protrusions in contact with the surface form the micro-cavities, which once in contact with the silicon oxide

(13) Kim, E.; Xia, Y.; Whitesides, G. M. *Nature* **1995**, *376*, 581.
(14) Messer, B.; Song, J. H.; Yang, P. D. *J. Am. Chem. Soc.* **2000**, *122*, 10232−10233.
(15) (a) Longoni, G.; Chini, P. J. *Am. Chem. Soc.* **1976**, *98*, 7225−7231. (b) Femoni, C.; Kaswalder, F.; Iapalucci, M. C.; Longoni, G.; Mehlstaubl, M.; Zacchini, S. *Chem. Commun.* **2005**, *46*, 5769−5771.
(16) Femoni, C.; Kaswalder, F.; Iapalucci, M. C.; Longoni, G.; Mehlstäubl, M.; Zacchini, S.; Ceriotti, A. *Angew. Chem., Int. Ed.* **2006**, *45*, 2060−2062.;

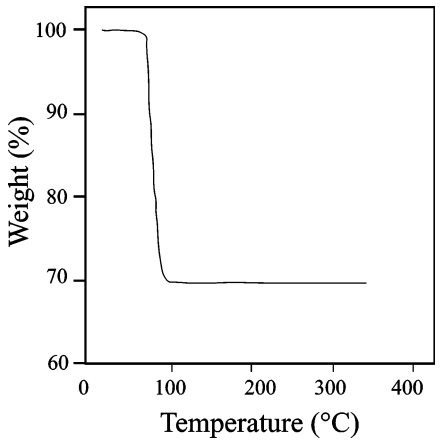

Figure 3. TGA of **1**. The weight becomes constant at ca. 70% of the original above 100 °C (theoretical Pt content for $[NBu_4]_2[Pt_{15}(CO)_{30}]$ is 68.8%).

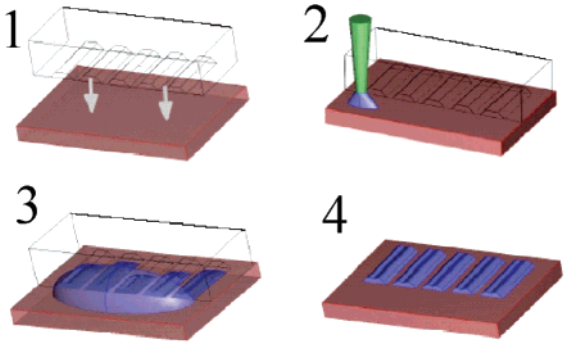

Figure 4. Scheme of microinject molding in capillaries.

substrate delimit the sub-micrometric channels (μ-channels). When the solution is poured at the open end of the stamp, the liquid spontaneously fills the μ-channels under the effect of capillary pressure. After the complete evaporation of the solvent (using DMF, 24 h at room temperature) the stamp is gently removed.

The self-organization of the solute enters into play at the later stages of shrinking, when the solution reaches supersaturation. Spatially organized nanodots or crystallites are fabricated by exploiting dewetting,[17] ripening, and crystallite growth.[18]

Finite Elements Simulation of the Microchannel Infilling. The infilling of PDMS-confined μ-channels is due to the capillary force and depends on surface tension and friction between the solvent and the channel walls.[19] Equating these contributions to pressure differences arising in the channel, it is possible to determine the local rate of flow, thus the time necessary to fill the microchannel. In this manner, it is possible to control the distance flown by the solution inside the channel

$$\mathrm{Re} \cdot f \cdot \frac{\eta \cdot w}{2 \cdot D_p^{\,2}} \cdot z = \frac{2 \cdot \sigma \cdot \cos(\theta)}{D_p} \qquad (1)$$

where Re is the Reynolds number, f, a geometrical factor, η, the viscosity of the solution, w, the velocity of the fluid along the main stream, σ, the surface tension, θ, the contact angle of the meniscus, and D_p, the wet perimeter of cross-section.

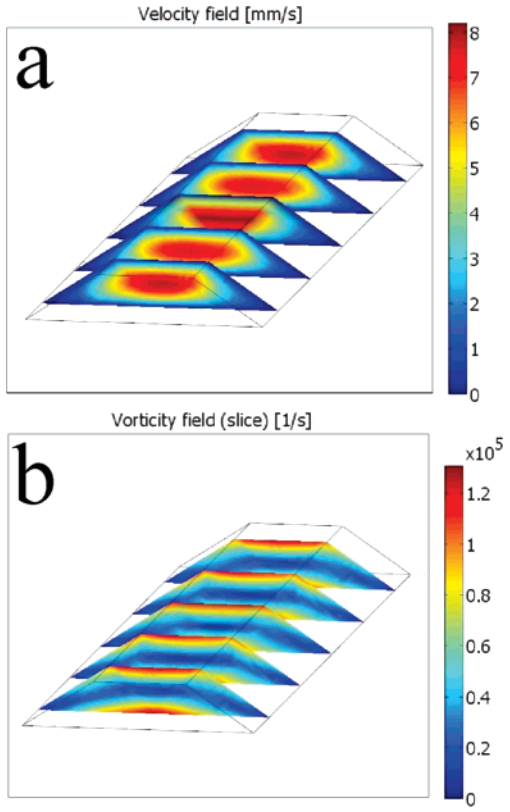

Figure 5. Finite elements simulation of the μ-channel infilling. (a) Velocity distribution for the main section of the μ-channels (mean value of 8 mm/s). (b) Vorticity distribution for the main section of the μ-channel.

Applying (eq 1) on a finite elements grid over the system domain we obtain a velocity field, which depends on the presence of the PDMS mold. The mean velocity calculated for our system is 8 mm/s which, using a stamp 6 mm length, corresponds to a time of infilling of 0.75 s. As depicted in Figure 5, the rate of the solution inside the microchannels is not constant but it tends to be faster in the center of the μ-channel with respect the border of the μ-channel. Furthermore, the simulation shows a high vorticity during the infilling (the vorticity is defined as $[(wy - vz)^2 + (uz - wx)^2 + (vx - uy)^2]^{1/2}$ where x, y, z are the spatial coordinates and u, v, w are the corresponding velocities), which indicate the laminar flux is distorted by geometry of the channel.[20] Although these effects are not intense enough to induce turbulence in the flux, they cause inhomogeneous distribution of the solute along the μ-channels when the solvent shrinks. In the range of concentration of 0 ÷ 1 g/L, no-relevant effect of solute or solvent shrinkage has been observed in the rheological properties.

As shown in Figure 6 μ-stripes of **1** exhibit birefringence under a polarized optical microscope, with domains (measured from power spectrum[1]) exceeding 20 μm.

The observation under crossed polars shows that the μ-stripes appear homogeneously colored. This indicates that their thickness is almost constant over the entire stripe. By rotating the microscope stage (viz. the crystal orientation vs the polarized light) the μ-stripes extinguished (became dark) in four positions

(17) (a) Cavallini, M.; Lazzaroni, R.; Zamboni, R.; Biscarini, F.; Timpel, D.; Zerbetto, F.; Clarkson, G. J.; Leigh D. A. *J. Phys. Chem. B* **2001**, *105*, 10826−10830. (b) Bystrenova, E.; Facchini, M.; Cavallini, M.; Cacace, M. G.; Biscarini, F. *Angew. Chem., Int. Ed.* **2006**, *45* (29), 4779−4782.
(18) Cavallini, M.; Facchini, M.; Massi, M.; Biscarini, F. *Synth. Met.* **2004**, *146*, 283.
(19) Nguyen, N. T.; Wereley, S. *Fundamentals and Applications of Microfluidics*; Artech House: Norwood, MA, 2002; Vol. 1.
(20) Chakraborty, S. *Appl. Phys. Lett.* **2007**, 034108.

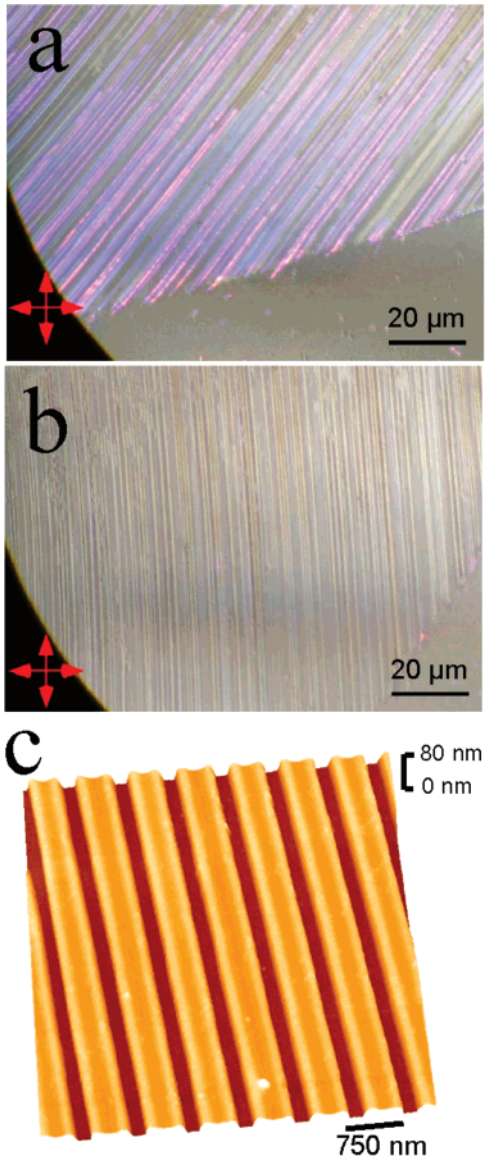

Figure 6. Optical micrographs of micrometric stripes fabricated on glass by MIMIC using $[NBu_4]_2[Pt_{15}(CO)_{30}]$ solutions (see details in the text) under nitrogen, with crossed polars. (a) Rotated ~30° with respect the polars and (b) parallel (perpendicular) to the polars. (c) Corresponding AFM images.

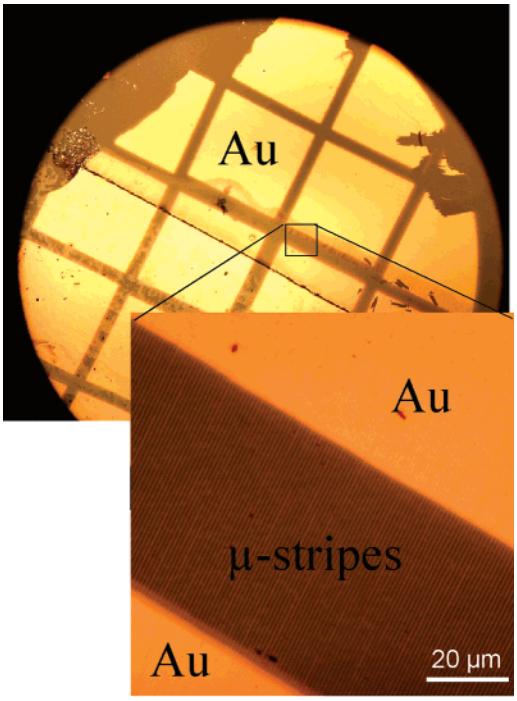

Figure 7. Optical micrographs of gold pads evaporated on μ-stripes.

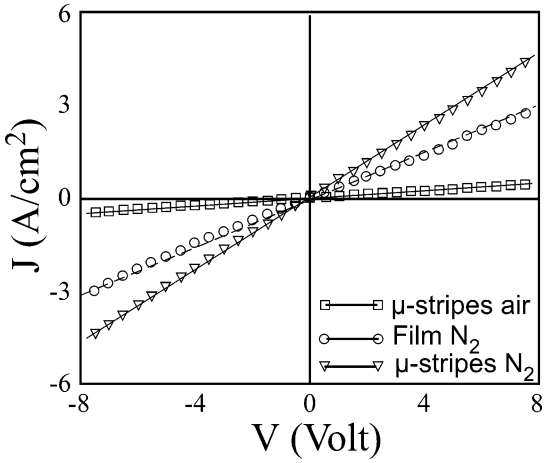

Figure 8. Current density−voltage characteristic of **1**: μ-stripes fabricated in air (□), drop cast film (○), and μ-stripes fabricated under nitrogen (△).

at intervals of 90° when the crossed polars were oriented parallel (perpendicular) to them while they are brightest when the crossed polars were oriented at 45°.

The occurrence of light extinction at the same orientations for all the domains indicates that the μ-stripes were grown with the same orientation. This means that the confined deposition has induced a coherent, long-range order along the direction of the stripes. As expected the stripes deposited in air do not exhibit birefringence.

Electrical Characterization. The electrical properties of the μ-stripes were studied using a two-probe configuration. Two gold pads to be used as electrodes were thermally evaporated on top of the pattern of μ-stripes through a square TEM grid (50 mesh) (Figure 7).

The length of the μ-stripes was measured using optical microscopy and the width and the thickness of the μ-stripes were measured analyzing the topography of the sample by AFM. It was observed by AFM and optical microscopy that not all the stripes are connected. It is thus relevant to consider the average number of stripes, which are connected, contributing to the current. The conductance of a single μ-stripe was calculated using the relationship $\kappa_{tot} = n \times \kappa_{single}$, where κ_{tot}, n, and κ_{single} are the conductance measured, average number of continuous stripes, and the conductance of each stripe, respectively.

Although a small percentage of the devices (~15%) exhibit an irreproducible non-ohmic I/V curve, all kinds of samples (i.e., prepared in air or under nitrogen and the annealed and as fabricated samples) show an ohmic behavior in the voltage range −8 V to +8 V but with a different electrical conductivity. Figure 8 shows the J/V curve of the μ-stripes fabricated in air and under nitrogen and the film prepared under nitrogen (the film prepared in air exhibit irreproducible behavior due to the higher number of defects).

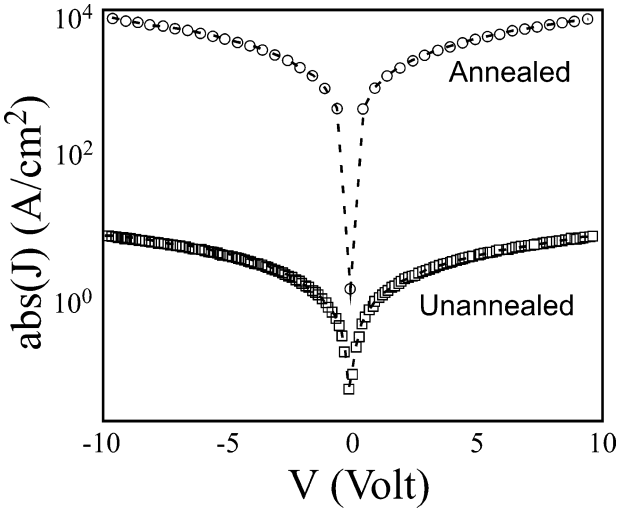

Figure 9. Comparison of current density−voltage characteristic of annealed and unannealed μ-stripes of $[NBu_4]_2[Pt_{15}(CO)_{30}]$ fabricated under nitrogen (current density is plotted on log scale).

Both the μ-stripes (fabricated in air protected by the stamp or fabricated under nitrogen) and the film drop cast under nitrogen exhibit an ohmic behavior in the voltage range −8 V to +8 V.

It is remarkable that the μ-stripes fabricated under nitrogen exhibit an electrical conductivity of $(2.1 \pm 1.5) \times 10^{-2}$ S/cm, which is 1 order of magnitude larger than that of the corresponding thin film ($\sim 1.0 \times 10^{-3}$ S/cm) grown by drop casting.

On the other hand, the μ-stripes fabricated in air (thus with a partial decomposition of the **1** during the process) exhibit a conductivity of $(7.1 \pm 1.5) \times 10^{-4}$ S/cm, thus more than 1 order of magnitude lower with respect to the stripes fabricated under nitrogen. The reason of lower electrical conductivity in the μ-stripes fabricated in air can be attributed to the high numbers of the defects (grains boundaries, cracks, etc.) generated during the partial decomposition of **1**. Furthermore, since the **1** decomposition is not complete, it gives rise to the formation of an ill-defined amorphous Pt-colloidal material highly contaminated by the organic products from the $[NBu_4]^+$ cations which are removed only upon thermal treatment. Conversely, the electrical conductivity is enhanced in the μ-stripes fabricated under nitrogen because they have a limited number of defects, resulting in a perfectly ordered crystalline material oriented along the direction of the μ-channel.

The deposition of the solute in a confined environment enhances long-range molecular order because the rate of deposition is slower (close to the quasi-equilibrium conditions) and the confinement depletes the number of stable nuclei that can be formed. As the lateral size of the channel is shorter than the characteristic length scales of nucleation and diffusion, ripening, and the lateral diffusivity of molecules are restricted, the stripes grow as a one-dimensional system, with a limited number of grain boundaries and defects, as already observed in other molecular systems such as organic semiconductors.[1]

Effect of Thermal Annealing on μ-Stripes. In the present case, a solution of platinum precursor in DMF was used. After preparation, the patterns were annealed in air at 150 °C for 2 h in order to achieve the complete decomposition of the carbonyl groups. Upon thermal annealing, the μ-stripes still exhibit an ohmic behavior (Figure 9) with an increase of the electrical conductivity to 34.6 ± 2.0 S/cm due to the decomposition of **1** to metallic platinum. Occasionally, after the annealing, small deviation from the ohmic behavior has been observed due to changes in the contact resistance between the gold pad and the Pt μ-stripes during annealing.

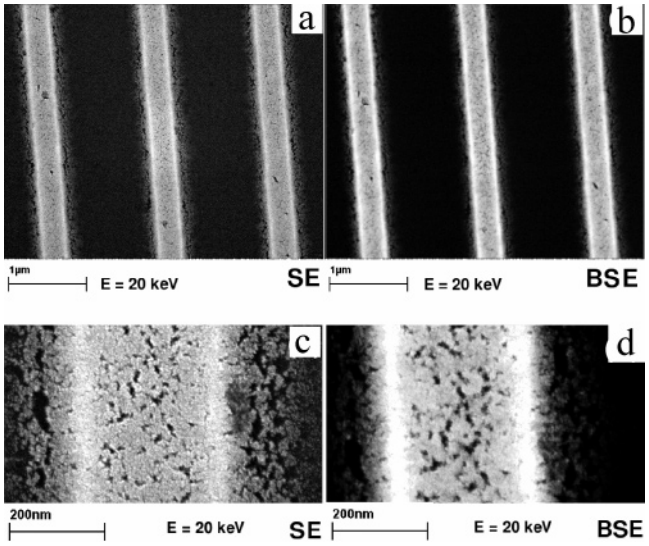

Figure 10. SEM images of Pt μ-stripes fabricated on Si: (a) a conventional secondary electron image; (b) obtained with a backscattered electrons detector, sensitive mainly to the sample composition; (c) zoom of a; (d) zoom of c.

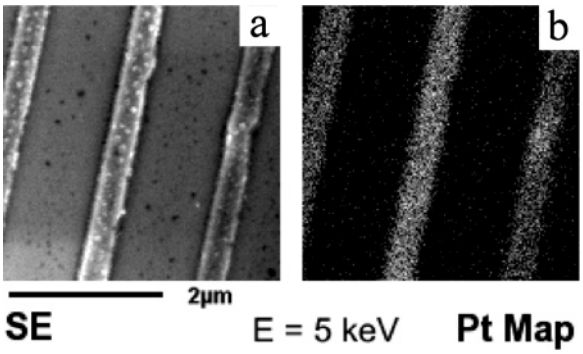

Figure 11. (a) Secondary electron image and (b) the corresponding X-ray map for Pt.

On the other hand, the μ-stripes fabricated in air (i.e., partially decomposed during the process) limit its increase of the electrical conductivity upon thermal annealing to 2.15 ± 1.0 S/cm, due to the presence of defects originated during the fabrication process.

Although the electrical conductivity of Pt wires obtained by our process is comparable to the electrical conductivity obtained in literature (80 S/cm at 20 °C),[2] this value is still far from the electrical conductivity of the bulk platinum ($\sim 10^5$ S/cm). In order to understand this difference, an accurate XRD and scanning Electron microscopy investigation of microannealed μ-stripes was done.

Scanning Electron Microscopy. In Figure 10 are reported two SEM images of the same portion of μ-stripes fabricated on Si, obtained with two different detectors. Figure 10a, c are Secondary Electron (SE) images obtained with an In-Lens detector, sensitive mainly to the topography of the stripes. They show the rough surface of the stripes and the presence of holes and grains of different size that form during the thermal

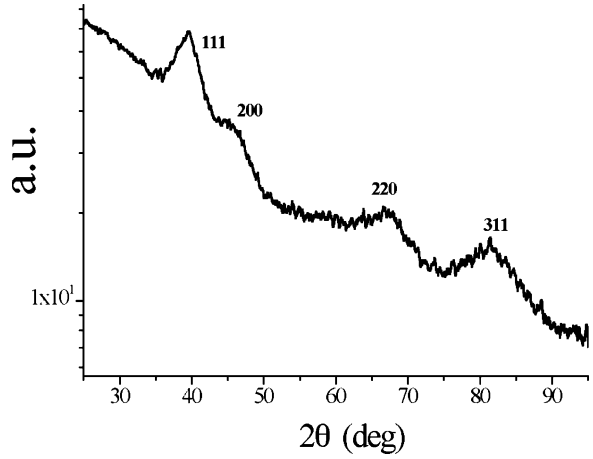

Figure 12. Diffraction pattern of the annealed film of **1** cast on glass. The Miller indexes, which correspond to the metallic Pt phase, have been reported.

treatment. Figure 10b, d are obtained with a BSE detector and shows mainly compositional information.

The μ-stripes show a bright contrast, as expected for a material with a high atomic number (Pt) on a substrate of low atomic number (Si). The roughness of the surface is still visible, but the uniform contrast along the stripe boundaries and inside the grains confirms the uniform composition of the stripes. These considerations are clearly confirmed by the results of the EDX measurements. In Figure 11 are reported a low-magnification secondary electron image (Figure 11a) and the corresponding X-ray map for Pt (Figure 11b), i.e., an image obtained collecting only the characteristic X-ray of the Pt emitted from the sample during the observation. As expected the Pt is localized inside the μ-stripes.

X-ray Diffraction. The structure of annealed films of **1** has been studied by X-ray diffraction measurements. The diffraction pattern has been recorded by using the grazing geometry, i.e., by keeping the incident beam at grazing angle on the sample surface, to enhance the scattering contribution from the surface. Figure 12 shows the pattern obtained on glass substrate, but the same results have been obtained on silicon covered by native oxide.

The films resulted formed by randomly oriented crystallites of cubic close-packed phase of the metallic Pt. The average coherent domain size, estimated from the FWHM (full width at half-maximum) of the peaks, is lower than 4 nm.

Conclusions

Here we showed the possibility to pattern ordered arrays of sub-micrometric stripes made from platinum-carbonyl clusters. This example illustrates the concept and application of a single-step bottom-up process that allows us to deposit size-defined stripes of a soluble molecular conductor. In this case long-range molecular order is achieved by solute deposition in a confined environment, because of slow deposition rate, hence quasi-equilibrium conditions, and lateral confinement that depletes the number of stable nuclei.[1]

In such a pattern electrical conductivity is enhanced and tuned by the control of size, shape, and order of the molecular domains: $[NBu_4]_2[Pt_{15}(CO)_{30}]$ μ-stripes exhibit an electrical conductivity of 2.1×10^{-2} S/cm, thus 4 orders of magnitude higher than that of the corresponding raw material (7.7×10^{-6} S/cm).[16]

Furthermore we showed that polycristaline Pt sub-micrometric wires can be obtained by thermal annealing of these $[NBu_4]_2[Pt_{15}(CO)_{30}]$ μ-stripes. Although this annealing process introduces morphological defects (grains and holes), electrical conductivity (35 S/cm) is found comparable to that of existing Pt or Pt/C composites nanowires (80 S/cm at 20 °C).

In the present study were used $[Pt_{15}(CO)_{30}]^{2-}$ clusters as representative material, but this process could be easily extended to any other soluble metal clusters. Furthermore, in order to fabricate functional devices, this technique could lead to the integration of Pt carbonyl clusters with other functional materials such as molecular magnets[21] or organic semiconductors[22] and combined with electrochemical systems.[23]

Acknowledgment. We thank Massimiliano Massi for stimulating discussions. This work was supported by "EU-Integrated Project NAIMO" (No NMP4-CT-2004-500355) and "PRRIITT NANOFABER". M.C. and P.S. are supported by ESF-EURYI -DYMOT. S.Q. is supported by Marie-Curie network CHEXTAN.

Supporting Information Available: (i) Materials and samples preparation. (ii) Characterization by Optical Microscopy, Atomic Force Microscopy, Scanning Electron Microscopy, X-ray Diffraction. (iii) Calculations regarding the Finite Element Modeling. This material is available free of charge via the Internet at http://pubs.as.org.

JA074104M

(21) Cavallini, M.; Albonetti, C.; Facchini, M.; Biscarini, F. *Phys. Chem. Chem. Phys.* **2008**, DOI:10.1039/b711677B.
(22) (a) Leclère, Ph.; Surin, M.; Cavallini, M.; Biscarini, F.; Lazzaroni, R. *Mater. Sci. Eng. R.* **2006**, *55*, 1−56. (b) Menozzi, C.; Corradini, V.; Cavallini, M.; Biscarini, F.; Betti, M.; Mariani, C. *Thin Solid films* **2003**, *428*, 227−231.
(23) Innocenti, M.; Cattarin, S.; Cavallini, M.; Loglio, F.; Foresti, M. L. *J. Electroanal. Chem.* **2002**, *532*, 219−225.